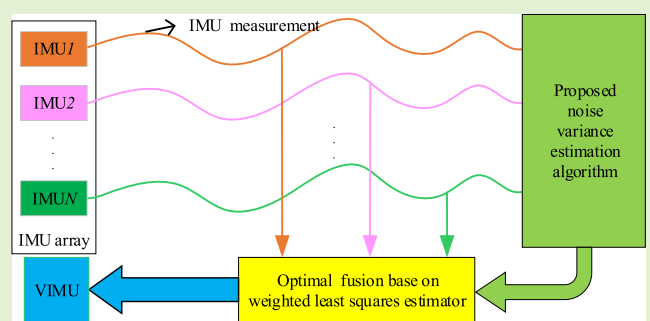


An Optimal Fusion Method of Multiple Inertial Measurement Units Based on Measurement Noise Variance Estimation

Hongliang Huang^{ID}, Hai Zhang^{ID}, and Liuyang Jiang^{ID}

Abstract—At present, most inertial systems generally only contain a single inertial measurement unit (IMU). Considering the low cost and low accuracy of the micro-electromechanical system (MEMS)-IMU, it has attracted much attention to fuse multiple IMUs to improve the accuracy and robustness of the system. In this article, two online noise variance estimators based on second-order-mutual-difference (SOMD) algorithm are proposed for two redundant measurements and multiple redundant measurements, respectively. In addition, the unbiasedness and consistency of the estimators are proved. Using the proposed noise variance estimators, measurement noise variances of each sensor can be estimated in real time when multiple IMUs exist. Based on the estimated noise variance of each sensor, the weighted least squares (WLS) estimation method is used to generate the optimal virtual IMU (VIMU) in the observation domain. Finally, comparative simulations and the real-world experiment were conducted to evaluate the proposed online noise estimation algorithm. The simulation results demonstrate its superiority compared with other noise variance estimation methods, and the real-world experiment results show the effectiveness of the IMU fusion method based on the proposed noise variance estimation algorithm.

Index Terms—Inertial measurement unit (IMU) fusion, noise variance estimation, redundant IMUs, second-order-mutual-difference (SOMD).



I. INTRODUCTION

WITH the development of hardware design and manufacturing, the cost and size of inertial measurement unit (IMU) based on micro-electromechanical system (MEMS) technology have been greatly reduced. As a result, MEMS-IMUs have been widely used in various applications, such as the vehicle positioning [1], [2], [3], virtual reality (VR) [4], augmented reality (AR) [5], etc. However, compared with the high-precision IMU, the reduction in the cost of the MEMS-IMU has also led to a drop in the performance. Though it can still provide remarkable accuracy in predicting short-term dynamic motion by measuring angular velocity and linear acceleration at high rates. Its accuracy will decrease in

the long time due to the complex noises contained in the raw measurements.

Considering the low cost and small size of the MEMS-IMU, it is possible to integrate multiple IMUs into the system to improve the robustness and accuracy of the system [6], [7]. Compared with a single IMU configuration, redundancy can improve the performance of the system in several aspects. First, sensors fault and spurious measurements can be detected and isolated, which improves the robustness of the system. Second, intrinsic noise can be estimated directly using the readings from the IMUs. Thus, the overall noise level can be reduced and the inertial measurements are closer to reality, which correspondingly improves the accuracy of system [8]. The performance of redundant IMUs and their potential benefits in inertial navigation have been studied in the past with higher order IMUs [9]. The experimental results with multiple MEMS-IMUs showed that the navigation performance could be improved by 30%–50% when using four IMUs [8]. Bancroft proposed a centralized filter method that fused multiple IMUs to generate the final navigation solutions in global positioning system (GPS) degraded areas. This method reduced the position drift in the outage of the GPS information using the relative updates between the IMUs [10]. Recently, multiple IMUs have also been used in visual-aided navigation. Eckenhoff et al. [11] proposed a real-time visual-inertial navi-

Manuscript received 28 October 2022; revised 30 November 2022; accepted 11 December 2022. Date of publication 20 December 2022; date of current version 31 January 2023. This work was supported by the National Key Research and Development Program of China under Grant 2017YFC0821102 and Grant 2016YFB0502004. The associate editor coordinating the review of this article and approving it for publication was Dr. Priyadip Ray. (*Corresponding author: Hai Zhang*)

Hongliang Huang and Hai Zhang are with the School of Automation Science and Electrical Engineering, Beihang University, Beijing 100191, China (e-mail: huanghl@buaa.edu.cn; zhanghai@buaa.edu.cn).

Liuyang Jiang is with the School of Information and Control Engineering, Qingdao University of Technology, Qingdao 266520, China (e-mail: jiangliuyang@qut.edu.cn).

Digital Object Identifier 10.1109/JSEN.2022.3229475

gation system (INS) that utilized the measurements from multiple IMUs. Like [10], the relative-pose constraints between the IMUs were utilized to mitigate the navigation drift accumulated over propagation. However, the proposed algorithm was computationally intensive, which is infeasible for low-computing platforms. Zhang et al. [12] proposed an algorithm for probabilistically fusing measurements from all the IMUs onto a virtual IMU (VIMU) through stochastic estimation with least-squares estimator and probabilistic marginalization of inter-IMU rotational accelerations. The experimental results showed that the performance of the fused IMU outperformed a single IMU.

In general, the redundant IMU fusion strategies can be divided into three categories: VIMU observation fusion method, the method based on centralized filter design, and the method based on federated filter design [13]. Compared with the other two methods, the VIMU observation fusion method requires less calculation and does not need to modify the existing INS and INS/GPS software since the redundant IMU output is synthesized into the usual IMU output. The prominent method of the observation fusion maps each IMU raw observations to the VIMU frame using least squares estimation. Theoretically, the optimal weight of each IMU is related to the measurement noise variance. However, the measurement noise of the same type of IMU is assumed to be the same in most literature. Then the least-squares estimation is just the average of all IMUs' measurements. The research in [14] showed that the assumption of assigning equal weights to all sensors was unreasonable since the noise powers across sensors might vary significantly. Though it is possible to estimate the noise of the sensor by some offline methods, such as Allan variance under static IMU condition, the noise level of the IMUs may evolve during the processing in response to particular situations (e.g., increase vibrations) [15]. The fixed noise parameters are also inappropriate during the whole process, which may lead to a suboptimal estimate of the fusing measurement, and even cause the divergence of the filter in severe cases. Therefore, the online noise variance estimation algorithm of MEMS-IMU is necessary. Guerrier [15] proposed a direct real-time estimation method of the VIMU process noise under the assumption that all the measurements had the same noise level. However, the algorithm could not estimate the noise variance of each sensor, and the assumption was unreasonable as mentioned above. Waegli et al. [14] applied the generalized autoregressive conditional heteroskedasticity (GARCH) [16] employed for studying the volatility of financial markets to estimate the variance for the individual sensors. However, this method is very complicated and requires more computational effort. In addition, the parameters used in the GARCH should be set carefully [14]. Another noise variance estimation method was proposed in [17], which could also achieve the noise variance estimate of a single IMU. However, it cannot track variance changes due to its algorithmic limitations. Meanwhile, when biases in the measurement model could not be ignored, the method would no longer be applicable. In [18], an online variance estimation method based on the minimum norm quadratic unbiased estimation (MINQUE) [19] was proposed, which can estimate the variances of sensors

at each time step. However, this method requires that the number of sensors is strictly greater than two times the number of signals to measure. In addition, similar to [17], it is also invalid when the baises of measurements exist. Recently, a relatively new noise estimation algorithm, second-order-mutual-difference (SOMD) algorithm, was proposed to estimate measurement noise variance in real time based on redundant measurements [20]. This method has been used in the adaptive Kalman filter to improve the stability and consistency of the filters [21], [22], [23], [24].

Considering the effectiveness and simplicity of the SOMD algorithm, in this article, two online variance estimators based on SOMD algorithm are proposed for two redundant measurements and multiple redundant measurements, respectively. And the detailed proof of the unbiasedness and consistency of the estimators are also provided. The optimal fusion of redundant IMU measurements is realized based on the weighted least squares (WLS) estimator using the estimated measurement noise variances, and the measurement equation of the VIMU is also derived. Finally, the proposed algorithms are validated in both simulations and real-world experiments.

The rest of this article is organized as follows. The noise variance estimators based on SOMD algorithm are proposed and the statistical properties of the estimators are studied in Section II. The VIMU generation method based on WLS estimation method are derived in detail in Section III. The performance of the proposed noise variance estimators is evaluated by both the simulation and real-world experiments in Section IV. Then we conclude the article.

II. NOISE VARIANCE ESTIMATION ALGORITHM

A. Motivation for Noise Variance Estimation

Let Z denote the true value of the signal to be estimated, and Z_1, \dots, Z_n be a set of n independent measurements with zero-mean white noise and the noise variance of the i th measurement is denoted as σ_i^2 . Theoretically, the optimal estimate \hat{Z} of the signal Z with the n independent measurements can be computed as a weighted average of them as

$$\hat{Z} = \sum_{i=1}^n w_i Z_i \quad \left(\sum_{i=1}^n w_i = 1 \right) \quad (1)$$

where w_i is the i th weight.

By linearity, we have $\mathbb{E}[\hat{Z}] = Z$ and since we assume $\text{Cov}(Z_i, Z_j) = 0$ for all $1 \leq i < j \leq n$, we have

$$\text{Var}(\hat{Z}) = \sigma^2 = \sum_{i=1}^n w_i^2 \sigma_i^2. \quad (2)$$

It can be seen from (2) that σ^2 is a multivariable quadric function of weights w_i ($i = 1, 2, \dots, n$). Then, the optimal fusion results can be obtained by minimizing the σ^2 subject to $\sum_{i=1}^n w_i = 1$. When σ^2 is minimized, the corresponding weights can be obtained by the constraint optimization method as

$$w_i^* = \frac{\frac{1}{\sigma_i^2}}{\sum_{i=1}^n \frac{1}{\sigma_i^2}} \quad (i = 1, 2, \dots, n). \quad (3)$$

Thus, σ^2 is

$$\sigma_{\min}^2 = \frac{1}{\sum_{i=1}^n \frac{1}{\sigma_i^2}}. \quad (4)$$

It can be seen from (3) that the weights are the function of the variances of all the measurements. Thus, it is essential to estimate the noise variance reasonably to obtain the optimal estimate of the signal.

B. SOMD Algorithm for Two Redundant Measurements

The SOMD algorithm was proposed to address the problem that the measurement noise variance in the Kalman filter cannot be effectively estimated. It can realize the real-time noise variance estimate of each measurement using the redundant measurements of the same signal. By constructing the first-order-self-difference (FOSD) of each measurement and SOMD between the measurements, it can eliminate the effect of the biases of each measurement and the changes in the observed signal on the estimate of noise variance.

Let $\mathbf{Z}_i(t)$ represent a measurement process which can be described as

$$\mathbf{Z}_i(t) = \mathbf{Z}(t) + \boldsymbol{\varepsilon}_i(t) + \mathbf{V}_i(t) \quad (5)$$

where $\mathbf{Z}(t) \in \mathbb{R}^q$ denotes the deterministic signal to be measured, $\boldsymbol{\varepsilon}_i(t) \in \mathbb{R}^q$ is the unknown bias which is modeled as the Gaussian random walk process, and $\mathbf{V}_i(t) \in \mathbb{R}^q$ is white Gaussian measurement noise. Then the following theorem holds.

Theorem 1: Assume that $\mathbf{Z}_1(t)$ and $\mathbf{Z}_2(t)$ are two independent measurement processes of the same signal $\mathbf{Z}(t)$. $\mathbf{Z}_1(k)$ and $\mathbf{Z}_2(k)$ are the samples of $\mathbf{Z}_1(t)$ and $\mathbf{Z}_2(t)$ at time $t = k\Delta t$ respectively, which can be given as

$$\begin{cases} \mathbf{Z}_1(k) = \mathbf{Z}(k) + \boldsymbol{\varepsilon}_1(k) + \mathbf{V}_1(k) \\ \mathbf{Z}_2(k) = \mathbf{Z}(k) + \boldsymbol{\varepsilon}_2(k) + \mathbf{V}_2(k) \end{cases} \quad (6)$$

where k is the discrete time index, Δt is the sampling period, $\mathbf{V}_1(k)$ and $\mathbf{V}_2(k)$ are mutually independent discrete noise and satisfy

$$\begin{cases} \mathbb{E}[\mathbf{V}_1(k)\mathbf{V}_1(j)^T] = \mathbf{R}_1\delta_{kj} \\ \mathbb{E}[\mathbf{V}_2(k)\mathbf{V}_2(j)^T] = \mathbf{R}_2\delta_{kj} \end{cases} \quad (7)$$

where δ_{kj} is the Kronecker delta function.

Then, the covariance matrix \mathbf{R}_1 and \mathbf{R}_2 can be expressed as

$$\begin{cases} \mathbf{R}_1 = \frac{\mathbb{E}[\nabla\mathbf{Z}_{12}(k)\nabla\mathbf{Z}_{12}(k)^T] + \mathbb{E}[\Delta\mathbf{Z}_1(k)\Delta\mathbf{Z}_1(k)^T]}{4} \\ - \frac{\mathbb{E}[\Delta\mathbf{Z}_2(k)\Delta\mathbf{Z}_2(k)^T]}{4} - \frac{\mathbb{E}[\Delta\boldsymbol{\varepsilon}_1(k)\Delta\boldsymbol{\varepsilon}_1(k)^T]}{2} \\ \mathbf{R}_2 = \frac{\mathbb{E}[\nabla\mathbf{Z}_{12}(k)\nabla\mathbf{Z}_{12}(k)^T] - \mathbb{E}[\Delta\mathbf{Z}_1(k)\Delta\mathbf{Z}_1(k)^T]}{4} \\ + \frac{\mathbb{E}[\Delta\mathbf{Z}_2(k)\Delta\mathbf{Z}_2(k)^T]}{4} - \frac{\mathbb{E}[\Delta\boldsymbol{\varepsilon}_2(k)\Delta\boldsymbol{\varepsilon}_2(k)^T]}{2} \end{cases} \quad (8)$$

where

$$\begin{cases} \Delta\mathbf{Z}_1(k) = \mathbf{Z}_1(k) - \mathbf{Z}_1(k-1) \\ \Delta\mathbf{Z}_2(k) = \mathbf{Z}_2(k) - \mathbf{Z}_2(k-1) \\ \nabla\mathbf{Z}_{12}(k) = \Delta\mathbf{Z}_1(k) - \Delta\mathbf{Z}_2(k) \\ \Delta\boldsymbol{\varepsilon}_1(k) = \boldsymbol{\varepsilon}_1(k) - \boldsymbol{\varepsilon}_1(k-1) \\ \Delta\boldsymbol{\varepsilon}_2(k) = \boldsymbol{\varepsilon}_2(k) - \boldsymbol{\varepsilon}_2(k-1). \end{cases} \quad (9)$$

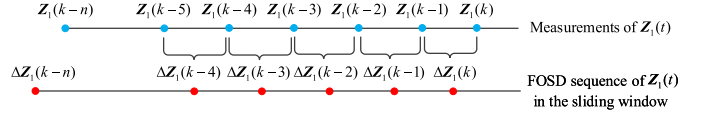


Fig. 1. Construction process of FOSD sequence of $\mathbf{Z}_1(t)$ in the sliding window.

Considering the limitation of the length of main context, the detailed proof of Theorem 1 is given in Appendix A-A.

In real applications, the noise covariance can be estimated approximately by utilizing the FOSD and SOMD samples. Then a sliding window is used to collect these samples as shown in Fig. 1 where the construction process of the FOSD sequence of $\mathbf{Z}_1(t)$ is demonstrated. The blue points represent the measurements at each sampling moment, and the red points denote the FOSD sample sequence in the sliding window. Based on the samples, estimators can be constructed as described by the following theorem.

Theorem 2: Assume that

$$\begin{cases} \mathbb{E}[\Delta\boldsymbol{\varepsilon}_1(k)\Delta\boldsymbol{\varepsilon}_1(j)^T] = \mathbf{Q}_1\delta_{kj} \\ \mathbb{E}[\Delta\boldsymbol{\varepsilon}_2(k)\Delta\boldsymbol{\varepsilon}_2(j)^T] = \mathbf{Q}_2\delta_{kj}. \end{cases} \quad (10)$$

Let

$$\begin{cases} \mathbf{L}_1 = \mathbf{R}_1 + \frac{\mathbf{Q}_1}{2} \\ \mathbf{L}_2 = \mathbf{R}_2 + \frac{\mathbf{Q}_2}{2}. \end{cases} \quad (11)$$

Based on (8), the estimators of \mathbf{L}_1 and \mathbf{L}_2 can be constructed as

$$\hat{\mathbf{L}}_1 = \frac{\boldsymbol{\mu}_{n2,\nabla\mathbf{Z}_{12}} - \boldsymbol{\mu}_{n2,\Delta\mathbf{Z}_2} + \boldsymbol{\mu}_{n2,\Delta\mathbf{Z}_1}}{4} \quad (12)$$

$$\hat{\mathbf{L}}_2 = \frac{\boldsymbol{\mu}_{n2,\nabla\mathbf{Z}_{12}} + \boldsymbol{\mu}_{n2,\Delta\mathbf{Z}_2} - \boldsymbol{\mu}_{n2,\Delta\mathbf{Z}_1}}{4} \quad (13)$$

where $\boldsymbol{\mu}_{n2,\mathbf{X}}$ is defined as

$$\boldsymbol{\mu}_{n2,\mathbf{X}} = \frac{1}{n} \sum_{i=1}^n \mathbf{X}_i \mathbf{X}_i^T \quad (14)$$

where n is the number of samples in the sliding window, and \mathbf{X}_i represents the i th sample in the sliding window. And the estimators are unbiased and weakly consistent.

The detailed proof of Theorem 2 is given in Appendix A-B.

Remark 1: In real applications, when the biases of measurements are constant, i.e.,

$$\begin{cases} \mathbb{E}[\Delta\boldsymbol{\varepsilon}_1(k)\Delta\boldsymbol{\varepsilon}_1(k)^T] = \mathbf{Q}_1 = \mathbf{0} \\ \mathbb{E}[\Delta\boldsymbol{\varepsilon}_2(k)\Delta\boldsymbol{\varepsilon}_2(k)^T] = \mathbf{Q}_2 = \mathbf{0}. \end{cases} \quad (15)$$

Then

$$\begin{cases} \mathbf{L}_1 = \mathbf{R}_1 \\ \mathbf{L}_2 = \mathbf{R}_2. \end{cases} \quad (16)$$

The discrete noise covariance \mathbf{R}_1 and \mathbf{R}_2 can be estimated with the proposed estimator. When the change of biases of measurements are extremely slow, i.e., the following conditions are met:

$$\begin{cases} \mathbb{E}[\Delta\boldsymbol{\varepsilon}_1(k)\Delta\boldsymbol{\varepsilon}_1(k)^T] \ll \mathbb{E}[\mathbf{V}_1(k)\mathbf{V}_1(k)^T] \\ \mathbb{E}[\Delta\boldsymbol{\varepsilon}_2(k)\Delta\boldsymbol{\varepsilon}_2(k)^T] \ll \mathbb{E}[\mathbf{V}_2(k)\mathbf{V}_2(k)^T]. \end{cases} \quad (17)$$

Then, the discrete noise covariance \mathbf{R}_1 and \mathbf{R}_2 can be estimated approximately with the proposed estimator ignoring the effect of \mathbf{Q}_1 and \mathbf{Q}_2 .

C. SOMD Algorithm for Multiple Redundant Measurements

The covariance estimator based on SOMD algorithm proposed above can be used to estimate the noise covariance when there are two redundant measurements. For the situation where multiple redundant measurements exist, to estimate noise covariance of each measurement, we can select any measurement as \mathbf{Z}_1 which is used as a reference, and any other measurement is selected as \mathbf{Z}_2 when its noise covariance needs to be estimated. By this way, the noise covariances of all measurements can be estimated with the proposed estimator. However, as mentioned above, in practice, the second raw moments of the FOSD sequence and SOMD sequence are estimated using the samples in the finite-length sliding window. These statistics cannot be exactly equal to their true value. As a result, when different measurement is selected as \mathbf{Z}_2 , the noise covariance estimates of \mathbf{Z}_1 are usually inconsistent. Especially when the statistics of the reference measurement deviate seriously from the true value, the noise variance estimates of all the measurements may be unreliable. To address these problems, a new covariance estimator based on SOMD algorithm is proposed when multiredundant measurements exist. Compared with the estimator above, the new estimator can realize the consistent noise covariance estimation of all the measurements. At the same time, it has better robustness and the formula is more concise.

Theorem 3: For a given system with n -independent measurements ($n \geq 3$) where the measurement equation can be described as (6) and (18), (shown at the bottom of the page), holds, where \mathbf{A}^+ is the Moore–Penrose inverse of the matrix \mathbf{A} .

The detailed proof of Theorem 3 is given in Appendix B-A.

Similar to the case where two redundant measurements exist, the noise covariance of each measurement can also be estimated approximately using the FOSD and SOMD samples in the sliding window when multiple redundant measurements exist. Thus, the following theorem is given.

Theorem 4: Assume that

$$\mathbb{E} [\Delta \boldsymbol{\varepsilon}_i(k) \Delta \boldsymbol{\varepsilon}_i(j)^T] = \mathbf{Q}_i \delta_{kj}, \quad (1 \leq i \leq n). \quad (19)$$

Let

$$\mathbf{L} = \begin{bmatrix} \mathbf{R}_1 \\ \mathbf{R}_2 \\ \mathbf{R}_3 \\ \vdots \\ \mathbf{R}_n \end{bmatrix} + \frac{1}{2} \mathbf{A}^+ \begin{bmatrix} \mathbf{Q}_1 + \mathbf{Q}_2 \\ \mathbf{Q}_1 + \mathbf{Q}_3 \\ \vdots \\ \vdots \\ \mathbf{Q}_{n-1} + \mathbf{Q}_n \end{bmatrix}. \quad (20)$$

Based on (18), the estimator of \mathbf{L} can be constructed as

$$\hat{\mathbf{L}} = \frac{1}{2} \mathbf{A}^+ \begin{bmatrix} \boldsymbol{\mu}_{n2, \nabla \mathbf{Z}_{12}} \\ \boldsymbol{\mu}_{n2, \nabla \mathbf{Z}_{13}} \\ \vdots \\ \boldsymbol{\mu}_{n2, \nabla \mathbf{Z}_{1n}} \\ \boldsymbol{\mu}_{n2, \nabla \mathbf{Z}_{23}} \\ \vdots \\ \boldsymbol{\mu}_{n2, \nabla \mathbf{Z}_{2n}} \\ \vdots \\ \vdots \\ \boldsymbol{\mu}_{n2, \nabla \mathbf{Z}_{(n-1)n}} \end{bmatrix}. \quad (21)$$

And the estimator is unbiased and weakly consistent.

The detailed proof of Theorem 4 is given in Appendix B-B.

Remark 2: In real applications, when the biases of all measurements are constant, i.e.,

$$\mathbb{E} [\Delta \boldsymbol{\varepsilon}_i(k) \Delta \boldsymbol{\varepsilon}_i(k)^T] = \mathbf{Q}_i = \mathbf{0}, \quad (1 \leq i \leq n). \quad (22)$$

Then

$$\mathbf{L} = \begin{bmatrix} \mathbf{R}_1 \\ \mathbf{R}_2 \\ \mathbf{R}_3 \\ \vdots \\ \mathbf{R}_n \end{bmatrix}. \quad (23)$$

The discrete noise covariance $\mathbf{R}_i, i = 1, \dots, n$ can be estimated with the proposed estimator. When the change of biases of measurements are extremely slow, the discrete

$$\begin{bmatrix} \mathbf{R}_1 \\ \mathbf{R}_2 \\ \mathbf{R}_3 \\ \vdots \\ \mathbf{R}_n \end{bmatrix} = \frac{1}{2} \mathbf{A}^+ \begin{bmatrix} \boldsymbol{\mu}_{2, \nabla \mathbf{Z}_{12}(k)} \\ \boldsymbol{\mu}_{2, \nabla \mathbf{Z}_{13}(k)} \\ \vdots \\ \boldsymbol{\mu}_{2, \nabla \mathbf{Z}_{1n}(k)} \\ \boldsymbol{\mu}_{2, \nabla \mathbf{Z}_{23}(k)} \\ \vdots \\ \boldsymbol{\mu}_{2, \nabla \mathbf{Z}_{2n}(k)} \\ \vdots \\ \vdots \\ \boldsymbol{\mu}_{2, \nabla \mathbf{Z}_{(n-1)n}(k)} \end{bmatrix} - \frac{1}{2} \mathbf{A}^+ \begin{bmatrix} \boldsymbol{\mu}_{2, \Delta \boldsymbol{\varepsilon}_1(k)} + \boldsymbol{\mu}_{2, \Delta \boldsymbol{\varepsilon}_2(k)} \\ \boldsymbol{\mu}_{2, \Delta \boldsymbol{\varepsilon}_1(k)} + \boldsymbol{\mu}_{2, \Delta \boldsymbol{\varepsilon}_3(k)} \\ \vdots \\ \boldsymbol{\mu}_{2, \Delta \boldsymbol{\varepsilon}_1(k)} + \boldsymbol{\mu}_{2, \Delta \boldsymbol{\varepsilon}_n(k)} \\ \boldsymbol{\mu}_{2, \Delta \boldsymbol{\varepsilon}_2(k)} + \boldsymbol{\mu}_{2, \Delta \boldsymbol{\varepsilon}_3(k)} \\ \vdots \\ \boldsymbol{\mu}_{2, \Delta \boldsymbol{\varepsilon}_2(k)} + \boldsymbol{\mu}_{2, \Delta \boldsymbol{\varepsilon}_n(k)} \\ \vdots \\ \vdots \\ \boldsymbol{\mu}_{2, \Delta \boldsymbol{\varepsilon}_{n-1}(k)} + \boldsymbol{\mu}_{2, \Delta \boldsymbol{\varepsilon}_n(k)} \end{bmatrix}, \quad \mathbf{A} = \begin{bmatrix} \mathbf{I}_q & \mathbf{I}_q & \mathbf{I}_q \\ \mathbf{I}_q & \ddots & \mathbf{I}_q \\ \vdots & & \vdots \\ \mathbf{I}_q & \mathbf{I}_q & \mathbf{I}_q \\ \vdots & & \vdots \\ \mathbf{I}_q & & \mathbf{I}_q \\ \vdots & & \ddots \\ & & \mathbf{I}_q & \mathbf{I}_q \end{bmatrix}_{\frac{(n-1)ng}{2} \times nq} \quad (18)$$

noise covariance $\mathbf{R}_i, i = 1, \dots, n$ can be estimated approximately with the proposed estimator ignoring the effect of $\mathbf{Q}_i, i = 1, \dots, n$.

In practice, to adapt to the variation of noise in time, the length of the sliding window should be limited. But the estimated noise variance of the measurement may jump suddenly due to insufficient samples. To ensure the smoothness of the variance, a fading memory calculation is implemented as below

$$\begin{cases} \hat{\mathbf{R}}_k = (1 - d_k) \mathbf{R}_{k-1} + d_k \mathbf{R}_k \\ d_k = \frac{1-b}{1-b^{k+1}} \end{cases} \quad (24)$$

where b is the fading factor, $0 < b < 1$.

III. OPTIMAL REDUNDANT IMUs FUSION

Considering that the proposed noise variance estimators can realize real-time noise variance estimation of all the measurements, the optimal weight of each measurement can be obtained directly based on the estimated variances. Based on this, the redundant IMU fusion method in the observation domain is used in this article, whereby the raw observations of each IMU are fused to generate a single VIMU measurement. The term VIMU is used here to describe the fusion architectures in the observation domain. By projecting each IMU's measurement to the VIMU frame $\{V\}$, we can estimate the noise variance of each IMU by the proposed noise variance estimation method. Then the optimal fusion of redundant IMU measurements can be realized with the WLS estimator using the estimated noise variances.

A. Virtual Gyro Generation

The gyro's measurements can be described by

$$\boldsymbol{\omega}_m = \boldsymbol{\omega}^I + \mathbf{b}_g + \mathbf{n}_g, \quad \mathbf{n}_g \sim \mathcal{N}(\mathbf{0}, \sigma_g^2 \mathbf{I}_3) \quad (25)$$

where $\boldsymbol{\omega}_m$ represents the gyro's measurements, $\{I\}$ represents the IMU frame, $\boldsymbol{\omega}^I$ is the angular velocity of the IMU expressed in the $\{I\}$ frame, \mathbf{b}_g is the measurement bias, and \mathbf{n}_g is the zero-mean white Gaussian noises. The bias \mathbf{b}_g can be approximated as a constant in a short time.

Assuming that N IMUs are fixed to a rigid body, their angular velocity readings may be different since they are expressed in different IMU frames. To estimate the measurement noise variances of the gyros, all the measurements must be projected to the same frame.

By projecting the gyro measurements to the VIMU frame, the following transformation can be obtained:

$$\boldsymbol{\omega}_m^V = \mathbf{R}_I^V \boldsymbol{\omega}_m^I \quad (26)$$

where \mathbf{R}_I^V is the direction cosine matrix from $\{I\}$ to $\{V\}$. Substituting (25) into (26) leads to

$$\begin{aligned} \boldsymbol{\omega}_m^V &= \mathbf{R}_I^V (\boldsymbol{\omega}^I + \mathbf{b}_g + \mathbf{n}_g) \\ &= \mathbf{R}_I^V \boldsymbol{\omega}^I + \mathbf{R}_I^V \mathbf{b}_g + \mathbf{R}_I^V \mathbf{n}_g \\ &= \boldsymbol{\omega}^V + \mathbf{b}_g^V + \mathbf{n}_g^V, \quad \mathbf{n}_g^V \sim \mathcal{N}(\mathbf{0}, \sigma_g^2 \mathbf{I}_3). \end{aligned} \quad (27)$$

It is noted that the mean and covariance matrix of the gyro noise are invariant upon rotations (proof:

$$\begin{aligned} \mathbb{E}[\mathbf{R}\mathbf{n}_g] &= \mathbf{R}\mathbb{E}[\mathbf{n}_g] = \mathbf{0} \text{ and } \mathbb{E}[(\mathbf{R}\mathbf{n}_g)(\mathbf{R}\mathbf{n}_g)^T] = \\ &\mathbf{R}\mathbb{E}[\mathbf{n}_g\mathbf{n}_g^T]\mathbf{R}^T = \mathbf{R}\sigma_g^2 \mathbf{I}_3 \mathbf{R}^T = \sigma_g^2 \mathbf{I}_3. \end{aligned}$$

In practical applications, the bias \mathbf{b}_g^V can be approximated as a constant in a short time. Compared with the measurement noise, the difference of the bias between every two adjacent moments can be neglected. Hence, the condition in (17) is well satisfied. Then the noise variances of gyros can be estimated with the proposed noise variance estimator when multiple measurements exist.

For the N IMUs, the following equation can be obtained:

$$\begin{bmatrix} \boldsymbol{\omega}_{m1} \\ \vdots \\ \boldsymbol{\omega}_{mN} \end{bmatrix} = \begin{bmatrix} \mathbf{R}_V^{I_1} \\ \vdots \\ \mathbf{R}_V^{I_N} \end{bmatrix} \boldsymbol{\omega}^V + \begin{bmatrix} \mathbf{b}_{g1} \\ \vdots \\ \mathbf{b}_{gN} \end{bmatrix} + \begin{bmatrix} \mathbf{n}_{g1} \\ \vdots \\ \mathbf{n}_{gN} \end{bmatrix}. \quad (28)$$

The optimal estimate of the virtual angular velocity based on WLS estimator can be expressed as

$$\hat{\boldsymbol{\omega}}^V = \arg \min_{\boldsymbol{\omega}} \left\| \begin{bmatrix} \boldsymbol{\omega}_{m1} \\ \vdots \\ \boldsymbol{\omega}_{mN} \end{bmatrix} - \begin{bmatrix} \mathbf{R}_V^{I_1} \\ \vdots \\ \mathbf{R}_V^{I_N} \end{bmatrix} \boldsymbol{\omega}^V - \begin{bmatrix} \mathbf{b}_{g1} \\ \vdots \\ \mathbf{b}_{gN} \end{bmatrix} \right\|_{\mathbf{W}^{-1}}^2 \quad (29)$$

where $\|\cdot\|_{\mathbf{W}^{-1}}^2$ is defined as $\|\mathbf{X}\|_{\mathbf{W}^{-1}}^2 = \mathbf{X}^T \mathbf{W}^{-1} \mathbf{X}$, \mathbf{W} is the covariance matrix of measurement noise of N gyros.

By solving (29), the estimate of virtual angular velocity can be given by

$$\hat{\boldsymbol{\omega}}^V = \mathbf{P}_H \begin{bmatrix} \boldsymbol{\omega}_{m1} \\ \vdots \\ \boldsymbol{\omega}_{mN} \end{bmatrix} - \mathbf{P}_H \begin{bmatrix} \mathbf{b}_{g1} \\ \vdots \\ \mathbf{b}_{gN} \end{bmatrix} \quad (30)$$

where

$$\mathbf{P}_H = (\mathbf{H}^T \mathbf{W}^{-1} \mathbf{H})^{-1} \mathbf{H}^T \mathbf{W}^{-1}, \quad \mathbf{H} = \begin{bmatrix} \mathbf{R}_V^{I_1} \\ \vdots \\ \mathbf{R}_V^{I_N} \end{bmatrix}. \quad (31)$$

In addition, by substituting (28) into (30), we obtain

$$\boldsymbol{\omega}^V - \hat{\boldsymbol{\omega}}^V = -\mathbf{P}_H \begin{bmatrix} \mathbf{n}_{g1} \\ \vdots \\ \mathbf{n}_{gN} \end{bmatrix}. \quad (32)$$

Then the measurement of virtual gyro can be given by combining (30) and (32) as

$$\boldsymbol{\omega}_{mV} = \boldsymbol{\omega}^V + \mathbf{b}_{gV} + \mathbf{n}_{gV}, \quad \mathbf{n}_{gV} \sim \mathcal{N}(\mathbf{0}, \mathbf{Q}_{gV}) \quad (33)$$

where $\boldsymbol{\omega}_{mV}$, \mathbf{b}_{gV} , and \mathbf{n}_{gV} are the measurement, bias, and noise of the virtual gyro respectively, and can be defined as

$$\begin{aligned} \boldsymbol{\omega}_{mV} &= \mathbf{P}_H \begin{bmatrix} \boldsymbol{\omega}_{m1} \\ \vdots \\ \boldsymbol{\omega}_{mN} \end{bmatrix}, \quad \mathbf{b}_{gV} = \mathbf{P}_H \begin{bmatrix} \mathbf{b}_{g1} \\ \vdots \\ \mathbf{b}_{gN} \end{bmatrix} \\ \mathbf{n}_{gV} &= \mathbf{P}_H \begin{bmatrix} \mathbf{n}_{g1} \\ \vdots \\ \mathbf{n}_{gN} \end{bmatrix}. \end{aligned} \quad (34)$$

B. Virtual Accelerometer Generation

Corresponding to (25), the measurement of the accelerometer can be given as

$$\mathbf{a}_m = \mathbf{R}_G^I (\mathbf{a}^G - \mathbf{g}^G) + \mathbf{b}_a + \mathbf{n}_a, \quad \mathbf{n}_a \sim \mathcal{N}(\mathbf{0}, \sigma_a^2 \mathbf{I}_3) \quad (35)$$

where $\{I\}$ and $\{G\}$ represent the IMU frame and global frame, respectively, \mathbf{a}_m is the accelerometer measurements, \mathbf{R}_G^I is the direction cosine matrix from $\{G\}$ to $\{I\}$, \mathbf{a}^G is the linear acceleration of the IMU expressed in frames $\{G\}$, \mathbf{b}_a is the bias, \mathbf{n}_a is the white Gaussian noises, and \mathbf{g}^G is the known gravity vector.

Different from (26), the transformation between the virtual accelerometer and the real accelerometer needs to consider the extra terms caused by the noncoincidence of their frame origins and the rotation of the rigid body. Let \mathbf{a}_I and \mathbf{a}_V represent the true acceleration at the origin of the frame $\{I\}$ and $\{V\}$, respectively, then the following equation holds:

$$\mathbf{a}_I^G = \mathbf{a}_V^G + \mathbf{R}_V^G (\boldsymbol{\omega}^V \times (\boldsymbol{\omega}^V \times \mathbf{p}_I^V)) + \mathbf{R}_V^G (\boldsymbol{\alpha}^V \times \mathbf{p}_I^V) \quad (36)$$

where $\boldsymbol{\omega}^V$, $\boldsymbol{\alpha}^V$ are the angular velocity and the angular acceleration of the rigid body expressed in the VIMU frame, respectively, and \mathbf{p}_I^V is the lever arm between the IMU and the VIMU frame origins.

The combination of (35) and (36) leads to

$$\begin{aligned} \mathbf{a}_{mI}^V &= \mathbf{R}_I^V \mathbf{a}_{mI} \\ &= \mathbf{R}_G^V (\mathbf{a}_V^G - \mathbf{g}^G) + (\boldsymbol{\omega}^V \times (\boldsymbol{\omega}^V \times \mathbf{p}_I^V)) \\ &\quad + (\boldsymbol{\alpha}^V \times \mathbf{p}_I^V) + \mathbf{R}_I^V \mathbf{b}_a + \mathbf{R}_I^V \mathbf{n}_a. \end{aligned} \quad (37)$$

It can be seen from (37) that the second and third terms on the right side include the lever arm vector, which may be different for each IMU. If we regard them as biases, the condition in (17) may not be satisfied. However, in practical applications, when the rotation maneuverability is not strong or the lever arm vectors from the IMUs to the VIMU are small, these two terms can be neglected [13]. Then the noise variance of the accelerometer can also be estimated with the proposed noise estimation method. Then the simplified virtual measurement can be written as

$$\mathbf{a}_{mV} \approx \mathbf{R}_G^V (\mathbf{a}_V^G - \mathbf{g}^G) + \mathbf{b}_{aV} + \mathbf{n}_{aV}, \quad \mathbf{n}_{aV} \sim \mathcal{N}(\mathbf{0}, \mathbf{Q}_{aV}) \quad (38)$$

where \mathbf{a}_{mV} , \mathbf{b}_{aV} , \mathbf{n}_{aV} are the measurement, bias, and noise of the virtual accelerometer, respectively, and can be defined as

$$\begin{aligned} \mathbf{a}_{mV} &= \mathbf{P}_H \begin{bmatrix} \mathbf{a}_{m1} \\ \vdots \\ \mathbf{a}_{mN} \end{bmatrix}, \quad \mathbf{b}_{aV} = \mathbf{P}_H \begin{bmatrix} \mathbf{b}_{a1} \\ \vdots \\ \mathbf{b}_{aN} \end{bmatrix} \\ \mathbf{n}_{aV} &= \mathbf{P}_H \begin{bmatrix} \mathbf{n}_{a1} \\ \vdots \\ \mathbf{n}_{aN} \end{bmatrix}. \end{aligned} \quad (39)$$

IV. EXPERIMENTS AND RESULTS

Both numerical simulations and real experiments were conducted to illustrate the effectiveness of the proposed algorithm. In the simulation, the proposed noise variance estimator based on the SOMD algorithm are compared with other noise variance estimation methods. In the real-world experiment, the noise estimation algorithm is applied to an IMU array board with five Bosch BMI088 IMUs to generate a VIMU by the redundant IMU fusion method. Then the VIMU is integrated into the GPS/INS/odometer integrated navigation algorithm with nonholonomic constraints for land vehicle [25]. The performance of the VIMU is evaluated using the dead reckoning position error of the vehicle under the condition of GPS outage.

A. Noise Variance Estimation Simulation

In this section, the comparative simulations with random weighting method [17] and MINQUE [18] were conducted to demonstrate the superiority of the proposed noise covariance estimation method.

Assume that the true value of the signal was generated by the following equation:

$$Z = \sin(2t) + \cos(t) + \log(0.5 + t/2) + 10 \quad (40)$$

which includes the trigonometric term, logarithmic term, and constant term. The measurement equation could be modeled as

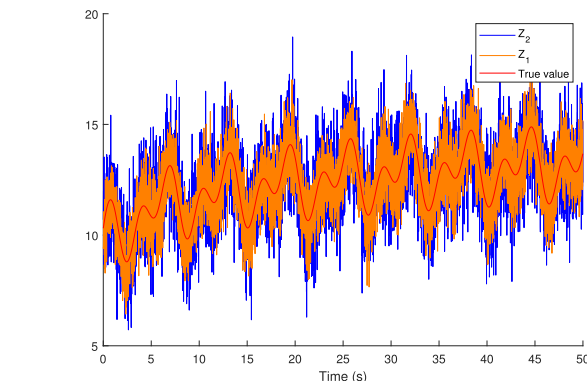
$$Z_i = Z + b_i + n_i, \quad (i = 1, \dots, 5) \quad (41)$$

where b_i and n_i represent the bias and the measurement noise of the i th measurement, and the bias is assumed to be constant in the simulation. The sampling frequency of the measurements is 100 Hz, and the total simulation time is 50 s.

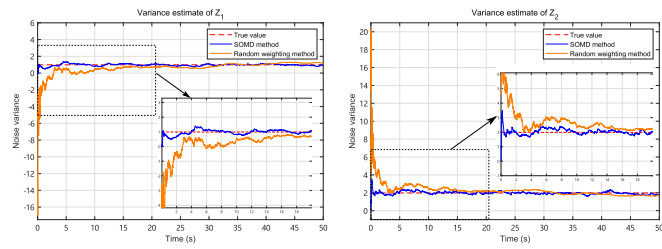
To evaluate the proposed noise estimation method in the case of two and multiple redundant measurements. The simulations were carried out in two different cases. In case 1, the number of measurements was two, the random weighting method and SOMD method were compared when the bias of each measurement was zero and nonzero, respectively. In addition, these two methods were also compared when the measurement noises were steady and time-varying, respectively. It should be noted that the MINQUE method was not compared in this case since it requires that the number of the measurements is strictly greater than twice the number of measured signals, i.e., the number of the measurement process is at least three. In case 2, the comparative simulations similar to case 1 were also conducted. But the number of measurements was increased to four.

Case 1: The number of measurements was two.

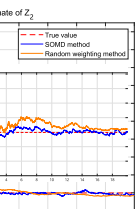
- 1) The bias of each measurement was set as zero, and the noise covariance remained unchanged during the simulation. Let σ_1^2 and σ_2^2 represent the discrete noise variance of these two measurements, respectively, which were set as $\sigma_1^2 = 1$, $\sigma_2^2 = 2$. The measurements and the true value of the signal are shown in Fig. 2(a). The noise variance estimate of each measurement with SOMD method and random weighting method are shown in



(a)



(b)

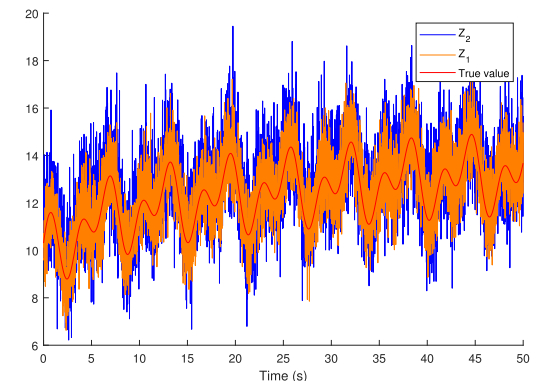


(c)

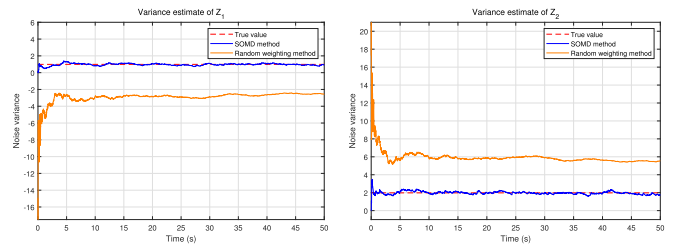
Fig. 2. Noise variance estimate of measurements by SOMD method and random weighting method. (a) Measured signal and the measurements of Z_1 , Z_2 with zero bias and constant noise variance. Variance estimate of (b) Z_1 and (c) Z_2 .

Fig. 2(b) and **(c)**, respectively. It can be seen from **Fig. 2** that the convergence time of variance estimation of random weighting method is much longer than that of SOMD method. One can also see that at the beginning of simulation, the estimation accuracy of the individual variances with the random weighting method is much lower than that of SOMD method, and the noise variance estimate with the random weighting method is unstable; even zero and negative value are obtained.

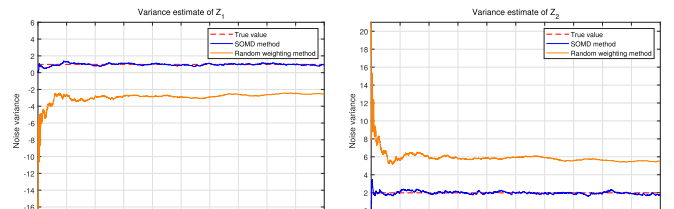
- 2) The noise variances remained unchanged during the simulation, but the bias of each measurement was set to nonzero. The values of σ_1^2 and σ_2^2 were set as the same as 1). And the biases of these two measurements b_1 and b_2 were set as $b_1 = 0.2$, $b_2 = 0.5$. The measurements and the true value of the signal are shown in **Fig. 3(a)**. The noise variance estimates of each measurement are shown in **Fig. 3(b)** and **(c)**, respectively. It can be seen that the biases have no effect on the noise variance estimation for the SOMD method. Instead, the random weighting method fails to estimate noise variance of each measurement when the biases of the measurement processes exist, which limits its application in practical applications.
- 3) The noise variances of the measurements were changed during the simulation to further investigate the ability of these two methods to estimate the time-varying noise. The noise variance of each measurement was changed during 20–40 s as shown in **Table I**. The bias of each measurement was set as zero. The simulation results are shown in **Fig. 4**, which illustrates that the estimated



(a)



(b)



(c)

Fig. 3. Noise variance estimate of measurements by SOMD method and random weighting method. (a) Measured signal and the measurements of Z_1 , Z_2 with nonzero bias and constant noise variance. Variance estimate of (b) Z_1 and (c) Z_2 .

TABLE I
NOISE VARIANCE OF TWO MEASUREMENTS OVER TIME

Time(s)	Z_1	Z_2
0–20s	1.00	2.00
20–40s	3.00	5.00
40–50s	1.00	2.00

TABLE II
NOISE VARIANCE OF FOUR MEASUREMENTS OVER TIME

Time(s)	Z_1	Z_2	Z_3	Z_4
0–20s	1.00	2.00	3.00	4.00
20–40s	3.00	5.00	6.00	1.00
40–50s	1.00	2.00	3.00	4.00

noise variance by the SOMD method can effectively track the true variance with a small delay, which depends on the factor b in (24). However, random weighting method cannot track variance changes due to its algorithmic limitations.

Case 2: The number of measurements was four.

- 1) The bias of each measurement process was set as zero, and the noise covariances remained unchanged during the simulation, which were set as $\sigma_1^2 = 1$, $\sigma_2^2 = 2$, $\sigma_3^2 = 3$, and $\sigma_4^2 = 4$, respectively. The noise variance estimates of each measurement with these three different methods are shown in **Fig. 5(a)–(d)**, respectively. One can see that the convergence time of SOMD method and MINQUE method are significantly shorter than that of random weighting method. Like case 1, the estimation accuracy of the individual variances with the random

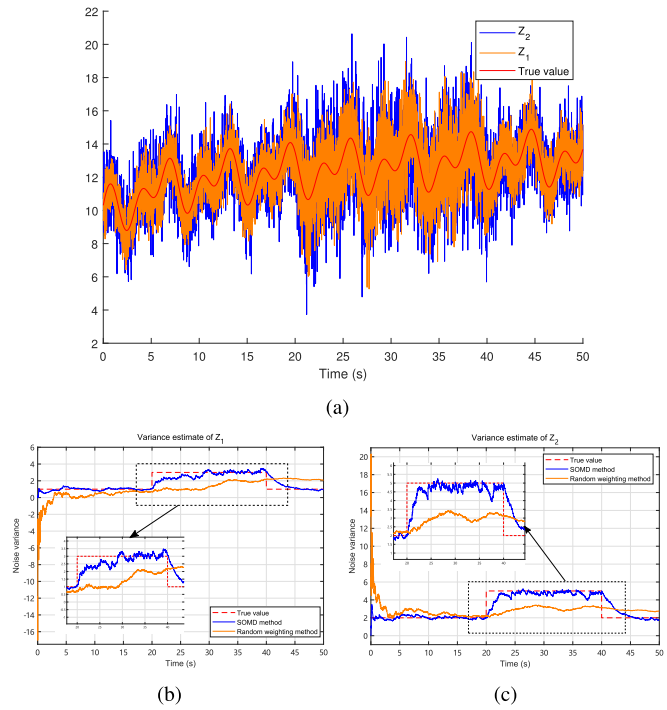


Fig. 4. Noise variance estimate of measurements by SOMD method and random weighting method. (a) Measured signal and the measurements of Z_1 , Z_2 with zero bias and time-varying noise variance. Variance estimate of (b) Z_1 and (c) Z_2 .

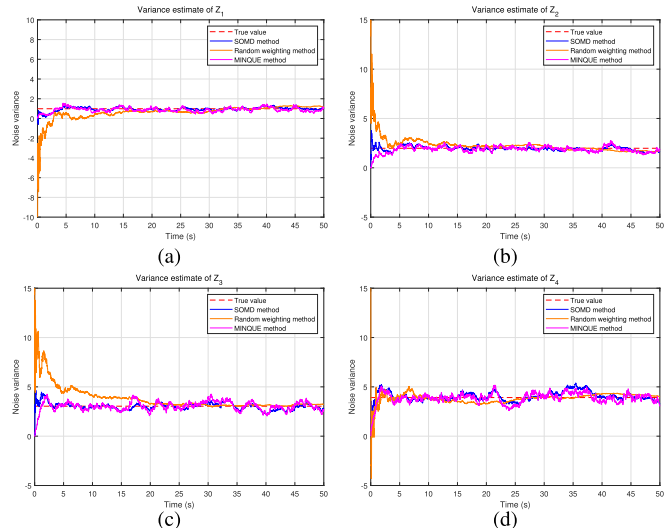


Fig. 5. Noise variance estimate of measurements with zero bias and constant noise variance. Variance estimate of (a) Z_1 , (b) Z_2 , (c) Z_3 , and (d) Z_4 .

weighting method is much lower than that of MINQUE method and SOMD method, and the estimated noise variance with the random weighting method is unstable.

- 2) The noise covariances remained unchanged during the simulation, but the biases were set randomly as $b_1 = 1$, $b_2 = 3$, $b_3 = 0.5$, $b_4 = 5$. In this case, only SOMD method and MINQUE method are compared since random weighting method has been shown to be invalid when biases exist in case 1. The simulation results are shown in Fig. 6. It can be seen

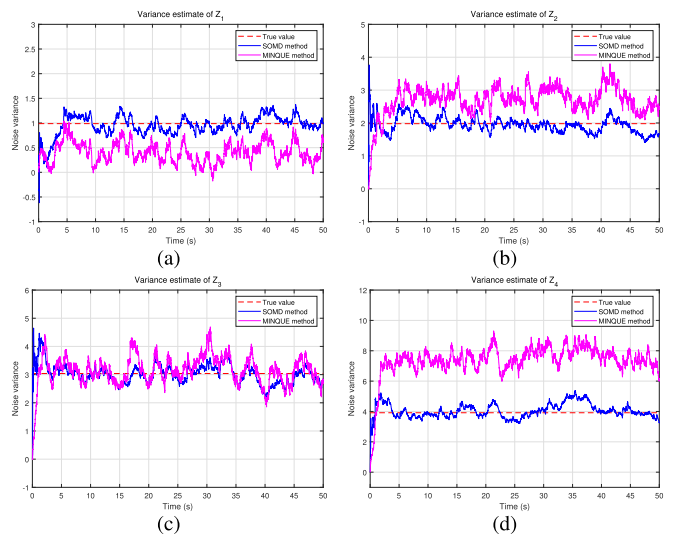


Fig. 6. Noise variance estimate of measurements with nonzero bias and constant noise variance. Variance estimate of (a) Z_1 , (b) Z_2 , (c) Z_3 , and (d) Z_4 .

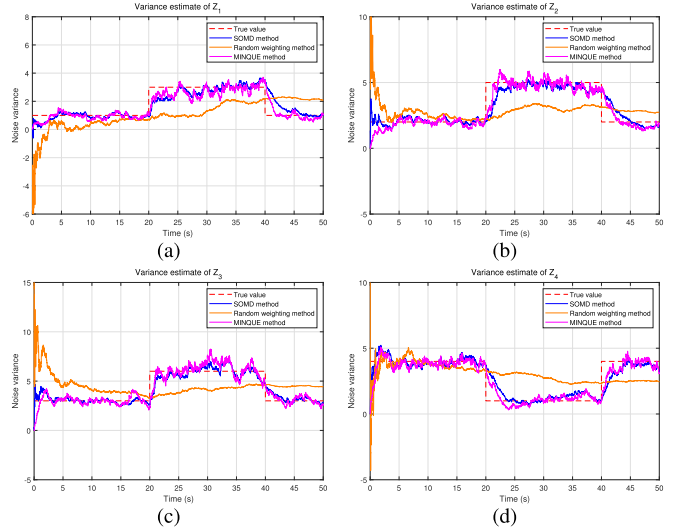


Fig. 7. Noise variance estimate of measurements with zero bias and time-varying noise variance. Variance estimate of (a) Z_1 , (b) Z_2 , (c) Z_3 , and (d) Z_4 .

that the MINQUE method cannot also estimate the noise variance of each measurement correctly like the random weighting method when the biases of the measurements exist. However, the SOMD method is still valid.

- 3) The bias of each measurement process was zero, but the noise variance of each measurement was changed during 20–40 s as shown in Table II. The simulation results are shown in Fig. 7. One can see that both the SOMD method and MINQUE method can track the variance change. But random weighting method is invalid in this case.

In general, when redundant measurements exist, compared with the other two methods, the SOMD method can effectively estimate the noise variance of each measurement regardless of whether the biases are zero. The estimation accuracy and the

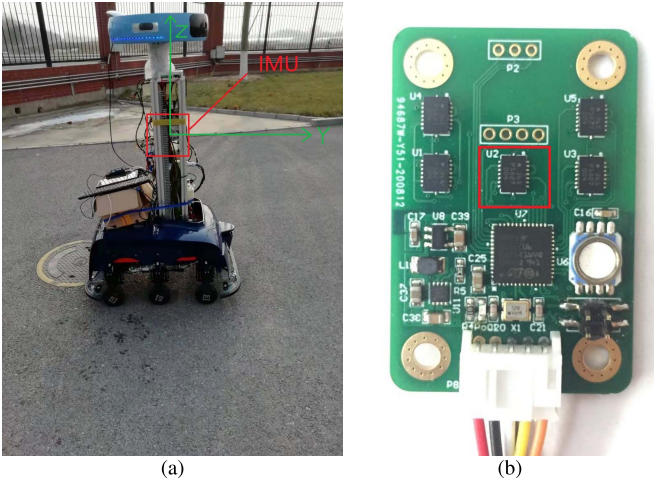


Fig. 8. Experiment setup. (a) Autonomous land robot. (b) IMU array board with five Bosch BMI088 IMUs.

stability of SOMD method are also the best. Compared with random weighting method, the SOMD method can effectively track the change of the noise variance, which can be used to estimate the time-varying noise. Compared with the MINQUE method, the SOMD method requires fewer measurements.

B. Real-World Experiment

To further evaluate the performance of the proposed noise estimation method in the real application of multiple IMUs fusion, the real-world experiments were conducted. The noise estimation methods used in the experiment include the Allan variance method, MINQUE method, and the proposed SOMD method. Furthermore, the novel scalewise variance optimization (SVO) method proposed in [27] is also compared here. The SVO method is a nonparametric method that utilizes the wavelet cross-covariance at different scales to combine the measurements coming from an array of sensors. Since weights are required for each of the scales, two different sets of weights are considered in this experiment, which are denoted as \mathbf{w}_1 and \mathbf{w}_2 , respectively. Specifically, \mathbf{w}_1 represents that the weights of the first half of scales are equal and the weights of the second half are set as zero. On the contrary, \mathbf{w}_2 represents that the weights of the first half of scales are set as zero and the weights of the second half are equal. It should be noted that the random weighting method was not used as a comparative method since we found the estimated noise variance of some IMUs with the method was negative in the real experiment.

The experimental setup consists of an autonomous robot equipped with a GPS-real-time kinematic (RTK) system, wheel speedometer and an IMU array board with five Bosch BMI088 IMUs, as shown in Fig. 8. The definition of the robot body frame $\{b\}$ is shown in Fig. 8(a). The X-axis points to the right side of the robot; the Y-axis points to the direction of the robot traveling; and the Z-axis points to the up direction. In the implementation of this experiment, the central IMU marked with a red rectangle in Fig. 8(b) on the board was selected to coincide with VIMU frame. The sampling frequency of IMU

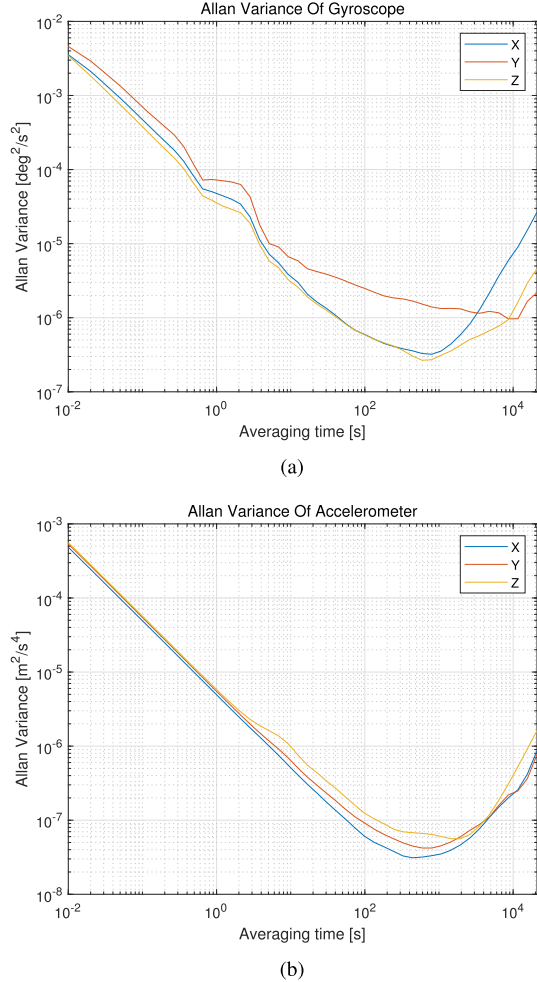
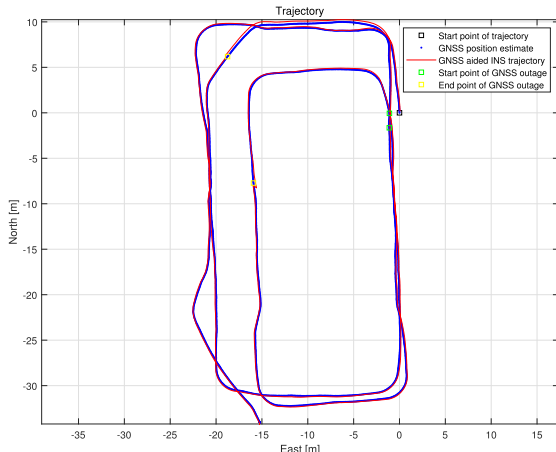


Fig. 9. Allan variance plot of IMU BMI088. Allan variance of (a) gyroscope and (b) accelerometer.

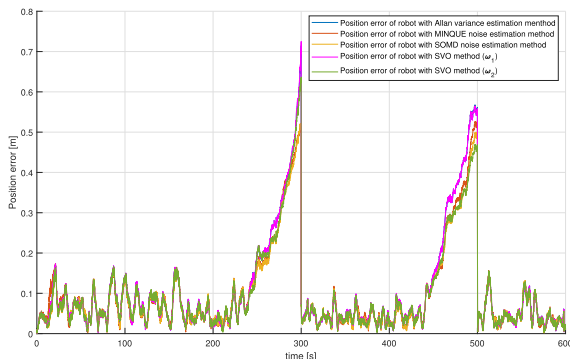
TABLE III
ESTIMATED DISCRETE NOISE VARIANCE OF GAUSSIAN WHITE NOISE
AND RANDOM WALK PROCESS IN THE ASSUMED MODEL OF
IMU FOR EACH AXIS

Axis	Gyroscope		Accelerometer	
	$\sigma_g^2(\text{deg}^2/\text{s}^2)$	$\gamma_g^2(\text{deg}^2/\text{s}^2)$	$\sigma_a^2(\text{m}^2/\text{s}^4)$	$\gamma_a^2(\text{m}^2/\text{s}^4)$
X	3.8866×10^{-3}	1.1854×10^{-11}	4.8645×10^{-4}	7.5947×10^{-13}
Y	5.1568×10^{-3}	3.4589×10^{-12}	5.3906×10^{-4}	8.4433×10^{-13}
Z	3.5692×10^{-3}	4.9890×10^{-12}	5.6213×10^{-4}	9.7850×10^{-13}

is 100 Hz. The 12 h of static data of the IMUs were collected and the Allan variance plot of one IMU is given in Fig. 9, where Fig. 9(a) and (b) illustrates the Allan variance plot of gyroscope and accelerometer, respectively. The discrete noise variances of Gaussian white noise and random walk processes in the assumed model of gyroscope and accelerometer are estimated using the generalized method of wavelet moments (GMWMs) proposed in [26]. Table III lists the estimated noise parameter values of gyroscope and accelerometer for each axis, where σ_g^2 and σ_a^2 represent the discrete noise variance of Gaussian white noise for gyroscope and accelerometer, respectively while γ_g^2 and γ_a^2 represent the discrete noise



(a)



(b)

Fig. 10. INS horizontal trajectory and the corresponding position error of Test #1. (a) INS trajectory. (b) Position error of fused IMU based on different methods.

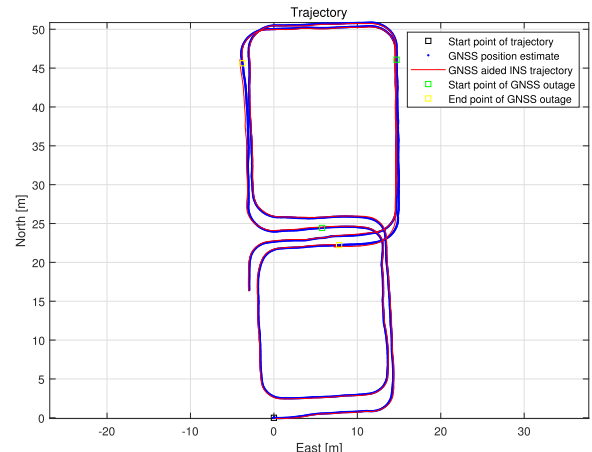
variance of Gaussian random walk processes for gyroscope and accelerometer, respectively. The RTK-fixed positioning solution output frequency was 5 Hz, the wheel speedometer output frequency was 20 Hz. All data were recorded with timestamp synchronization. The RTK-fixed positioning solution was used as the ground truth of the robot's position.

To test the performance of the VIMU under different driving conditions, two different driving trajectories were tested in the open-sky areas, as shown in Figs. 10(a) and 11(a). Considering the specific application scenarios of the autonomous robot for factory inspections, its driving area was limited. Therefore, the GPS position coordinates of the robot were converted to the Universal Transverse Mercator (UTM) coordinates. The fixed local east-north-up (ENU) coordinates system was defined as the navigation frame $\{n\}$ and the starting point of the trajectory was chosen as the origin of frame $\{n\}$. Since the low-cost IMU cannot sense the rotation of the earth, the frame $\{n\}$ could be regarded as an inertial reference frame ignoring the earth's rotation.

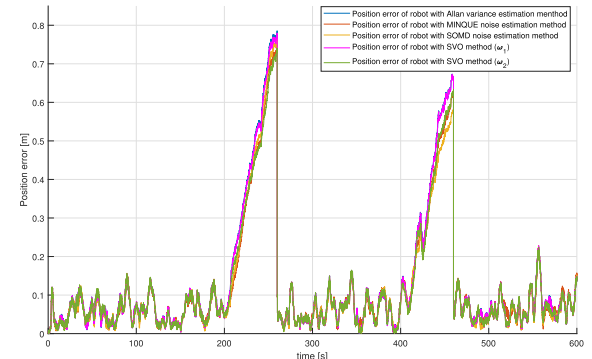
The performance of the fused IMU is evaluated using the dead reckoning position error under the condition of the GPS outage, which is defined as

$$e = \sqrt{(\hat{x} - x_{\text{rtk}})^2 + (\hat{y} - y_{\text{rtk}})^2 + (\hat{z} - z_{\text{rtk}})^2} \quad (42)$$

where $(x_{\text{rtk}}, y_{\text{rtk}}, z_{\text{rtk}})$ is the robot's position obtained from the RTK receiver, and $(\hat{x}, \hat{y}, \hat{z})$ is the estimated robot's position



(a)



(b)

Fig. 11. INS horizontal trajectory and the corresponding position error of Test #2. (a) INS trajectory. (b) Position error of fused IMU based on different methods.

TABLE IV
RMSE OF THE POSITION DURING THE GPS OUTAGE

Method	Test #1 (m)	Test #2 (m)
The Allan variance method	0.3425	0.4501
The MINQUE method	0.3057	0.4107
The SOMD method	0.2947	0.4103
The SVO method (w_1)	0.3431	0.4468
The SVO method (w_2)	0.3044	0.4091

from the integrated navigation algorithm. To mimic the loss of the satellite signals, 1 min of the RTK-fixed position data outage is deliberately added into the integrated navigation algorithm. As shown in Figs. 10(a) and 11(a), the starting points of every GPS outage are marked with green squares, the endpoints are marked with yellow squares, and the horizontal position of the robot from the navigation algorithm is plotted with the red lines. The corresponding position error of the robot based on the VIMU fused by different methods is shown in Figs. 10(b) and 11(b), respectively. In addition, the root-mean-square error (RMSE) of the position during the GPS outage was also computed as the statistic comparison, as shown in Table IV.

It can be seen from Figs. 10(b) and 11(b), and Table IV that the experimental results of the other methods are at least

as good as the Allan variance method. In particular, the performance of SOMD method and MINQUE method are nearly identical to SVO method with w_2 . Though the results of these methods are comparable, there are some differences among them. On the one hand, the SOMD method proposed in this article relies on strong parametric assumptions where both the white noise process and the random walk process are assumed to be Gaussian. These underlying parameter assumptions may not always hold in real applications, especially for the low-cost MEMS IMUs with more complex stochastic structures. In contrast, the Allan variance-based methods and SVO method rely on weaker parametric assumptions and in particular the SVO method is a fully nonparametric method that does not rely on any parametric assumption on the stochastic processes of the individual signals, which provides considerable advantages in real-world applications. Moreover, the SVO method is flexible as the weight vector used for different wavelet scales can be set by the users according to practical application requirements for inertial sensor calibration. On the other hand, the main advantage of the SOMD method resides in the fact that it is adaptive and can adapt to changes of the noise characteristics, which is suitable for the case where the noise level of the MEMS-IMUs may evolve due to the external environmental influences such as the vibration, whereas this is not possible with the Allan variance-based methods and SVO method.

In general, all methods have their advantages and own limitations due to arguably unrealistic assumptions. In practice, it is difficult to know if weaker parametric assumptions are better or worse than adaptive capabilities. However, it is interesting to incorporate these ideas in the future research to open new research directions where nonparametric methods (such as the SVO method) with adaptive capabilities (such as the SOMD method) could be developed.

V. CONCLUSION

In this article, two online noise variance estimators based on SOMD algorithm are proposed for two redundant measurements and multiple redundant measurements, respectively. The detailed proof of the unbiasedness and consistency of the estimators are also provided. Using the proposed noise variance estimator, the measurement noise variances of each IMU sensor can be estimated in real time when multiple IMUs exist. Based on the estimated noise variances of each sensor, the measurement equation of the optimal VIMU in the observation domain by the WLS estimation method is derived. Finally, the performance of the proposed noise variance estimation algorithm was verified through comparative simulations with random weighting method, MINQUE method. The results demonstrate the superiority of the proposed noise variance estimation on steady noise and time-varying noise regardless of whether there are measurement biases. Meanwhile, the real-world experiment was also implemented to evaluate the performance of the generated VIMU based on different methods such as Allan variance, MINQUE method, and the SVO method. The experimental results show the effectiveness of the IMU fusion method based on the proposed noise variance estimation algorithm and the performance of the VIMU is comparable to the other methods.

APPENDIX A

PROOFS OF THEOREMS IN SECTION II-B

In this appendix, we provide the detailed proofs of Theorems 1 and 2 in Section II-B considering the limitation of the length of the main context in the article.

A. Proof of Theorem 1

Proof: The FOSD items $\Delta\mathbf{Z}_1(k)$ and $\Delta\mathbf{Z}_2(k)$ of each measurement process at time index k can be obtained by taking the difference of measurements at two adjacent sampling moments as

$$\begin{aligned}\Delta\mathbf{Z}_1(k) &= \mathbf{Z}_1(k) - \mathbf{Z}_1(k-1) \\ &= \mathbf{Z}(k) - \mathbf{Z}(k-1) + \boldsymbol{\varepsilon}_1(k) - \boldsymbol{\varepsilon}_1(k-1) \\ &\quad + \mathbf{V}_1(k) - \mathbf{V}_1(k-1) \\ &= \Delta\mathbf{Z}(k) + \Delta\boldsymbol{\varepsilon}_1(k) + \mathbf{V}_1(k) - \mathbf{V}_1(k-1) \\ \Delta\mathbf{Z}_2(k) &= \mathbf{Z}_2(k) - \mathbf{Z}_2(k-1) \\ &= \mathbf{Z}(k) - \mathbf{Z}(k-1) + \boldsymbol{\varepsilon}_2(k) - \boldsymbol{\varepsilon}_2(k-1) \\ &\quad + \mathbf{V}_2(k) - \mathbf{V}_2(k-1) \\ &= \Delta\mathbf{Z}(k) + \Delta\boldsymbol{\varepsilon}_2(k) + \mathbf{V}_2(k) - \mathbf{V}_2(k-1).\end{aligned}\quad (43)$$

Correspondingly, the SOMD item $\nabla\mathbf{Z}_{12}(k)$ at time index k can be given by taking the difference of these two FOSD items $\Delta\mathbf{Z}_1(k)$ and $\Delta\mathbf{Z}_2(k)$ as

$$\begin{aligned}\nabla\mathbf{Z}_{12}(k) &= \Delta\mathbf{Z}_1(k) - \Delta\mathbf{Z}_2(k) \\ &= \Delta\mathbf{Z}(k) + \Delta\boldsymbol{\varepsilon}_1(k) + (\mathbf{V}_1(k) - \mathbf{V}_1(k-1)) \\ &\quad - \Delta\mathbf{Z}(k) - \Delta\boldsymbol{\varepsilon}_2(k) - (\mathbf{V}_2(k) - \mathbf{V}_2(k-1)) \\ &= \Delta\boldsymbol{\varepsilon}_1(k) - \Delta\boldsymbol{\varepsilon}_2(k) + (\mathbf{V}_1(k) - \mathbf{V}_1(k-1)) \\ &\quad - (\mathbf{V}_2(k) - \mathbf{V}_2(k-1)).\end{aligned}\quad (44)$$

Let $\boldsymbol{\mu}_{m,\mathbf{X}}$ denote the m th raw moment of the random vector \mathbf{X} . Then the first raw moments of $\Delta\mathbf{Z}_1(k)$, $\Delta\mathbf{Z}_2(k)$, and $\nabla\mathbf{Z}_{12}(k)$ can be given as

$$\begin{aligned}\boldsymbol{\mu}_{1,\Delta\mathbf{Z}_1(k)} &= \mathbb{E}[\Delta\mathbf{Z}_1(k)] = \Delta\mathbf{Z}(k) \\ \boldsymbol{\mu}_{1,\Delta\mathbf{Z}_2(k)} &= \mathbb{E}[\Delta\mathbf{Z}_2(k)] = \Delta\mathbf{Z}(k) \\ \boldsymbol{\mu}_{1,\nabla\mathbf{Z}_{12}(k)} &= \mathbb{E}[\nabla\mathbf{Z}_{12}(k)] = \mathbf{0}.\end{aligned}\quad (45)$$

And the second raw moments of these items can be obtained as

$$\begin{aligned}\boldsymbol{\mu}_{2,\Delta\mathbf{Z}_1(k)} &= \mathbb{E}[\Delta\mathbf{Z}_1(k)\Delta\mathbf{Z}_1(k)^T] \\ &= \Delta\mathbf{Z}(k)\Delta\mathbf{Z}(k)^T + \mathbb{E}[\Delta\boldsymbol{\varepsilon}_1(k)\Delta\boldsymbol{\varepsilon}_1(k)^T] \\ &\quad + \mathbb{E}[\mathbf{V}_1(k)\mathbf{V}_1(k)^T] + \mathbb{E}[\mathbf{V}_1(k-1)\mathbf{V}_1(k-1)^T] \\ &= \Delta\mathbf{Z}(k)\Delta\mathbf{Z}(k)^T + \mathbb{E}[\Delta\boldsymbol{\varepsilon}_1(k)\Delta\boldsymbol{\varepsilon}_1(k)^T] + 2\mathbf{R}_1\end{aligned}\quad (46)$$

$$\begin{aligned}\boldsymbol{\mu}_{2,\Delta\mathbf{Z}_2(k)} &= \mathbb{E}[\Delta\mathbf{Z}_2(k)\Delta\mathbf{Z}_2(k)^T] \\ &= \Delta\mathbf{Z}(k)\Delta\mathbf{Z}(k)^T + \mathbb{E}[\Delta\boldsymbol{\varepsilon}_2(k)\Delta\boldsymbol{\varepsilon}_2(k)^T] \\ &\quad + \mathbb{E}[\mathbf{V}_2(k)\mathbf{V}_2(k)^T] + \mathbb{E}[\mathbf{V}_2(k-1)\mathbf{V}_2(k-1)^T] \\ &= \Delta\mathbf{Z}(k)\Delta\mathbf{Z}(k)^T + \mathbb{E}[\Delta\boldsymbol{\varepsilon}_2(k)\Delta\boldsymbol{\varepsilon}_2(k)^T] + 2\mathbf{R}_2\end{aligned}\quad (47)$$

$$\begin{aligned}
& \mu_{2,\nabla Z_{12}(k)} \\
&= \mathbb{E} \left[\nabla Z_{12}(k) \nabla Z_{12}(k)^T \right] \\
&= \mathbb{E} \left[\Delta \boldsymbol{\varepsilon}_1(k) \Delta \boldsymbol{\varepsilon}_1(k)^T \right] + \mathbb{E} \left[\Delta \boldsymbol{\varepsilon}_2(k) \Delta \boldsymbol{\varepsilon}_2(k)^T \right] \\
&\quad + \mathbb{E} \left[\mathbf{V}_1(k) \mathbf{V}_1(k)^T \right] + \mathbb{E} \left[\mathbf{V}_1(k-1) \mathbf{V}_1(k-1)^T \right] \\
&\quad + \mathbb{E} \left[\mathbf{V}_2(k) \mathbf{V}_2(k)^T \right] + \mathbb{E} \left[\mathbf{V}_2(k-1) \mathbf{V}_2(k-1)^T \right] \\
&= \mathbb{E} \left[\Delta \boldsymbol{\varepsilon}_1(k) \Delta \boldsymbol{\varepsilon}_1(k)^T \right] + \mathbb{E} \left[\Delta \boldsymbol{\varepsilon}_2(k) \Delta \boldsymbol{\varepsilon}_2(k)^T \right] \\
&\quad + 2\mathbf{R}_1 + 2\mathbf{R}_2. \tag{48}
\end{aligned}$$

Let (47) subtract (46), the following equation can be obtained:

$$\begin{aligned}
\mu_{2,\Delta Z_2(k)} - \mu_{2,\Delta Z_1(k)} &= 2\mathbf{R}_2 - 2\mathbf{R}_1 + \mathbb{E} \left[\Delta \boldsymbol{\varepsilon}_2(k) \Delta \boldsymbol{\varepsilon}_2(k)^T \right] \\
&\quad - \mathbb{E} \left[\Delta \boldsymbol{\varepsilon}_1(k) \Delta \boldsymbol{\varepsilon}_1(k)^T \right]. \tag{49}
\end{aligned}$$

Let (48) subtract (49), \mathbf{R}_1 can be expressed as

$$\begin{aligned}
\mathbf{R}_1 &= \frac{\mu_{2,\nabla Z_{12}(k)} - \mu_{2,\Delta Z_2(k)} + \mu_{2,\Delta Z_1(k)}}{4} \\
&\quad - \frac{\mathbb{E} \left[\Delta \boldsymbol{\varepsilon}_1(k) \Delta \boldsymbol{\varepsilon}_1(k)^T \right]}{2}. \tag{50}
\end{aligned}$$

Similarly, let (48) add (49), \mathbf{R}_2 can be expressed as

$$\begin{aligned}
\mathbf{R}_2 &= \frac{\mu_{2,\nabla Z_{12}(k)} + \mu_{2,\Delta Z_2(k)} - \mu_{2,\Delta Z_1(k)}}{4} \\
&\quad - \frac{\mathbb{E} \left[\Delta \boldsymbol{\varepsilon}_2(k) \Delta \boldsymbol{\varepsilon}_2(k)^T \right]}{2}. \tag{51}
\end{aligned}$$

■

B. Proof of Theorem 2

Proof: The proof of the unbiasedness of the estimators is given as follows.

By taking the expectation of $\hat{\mathbf{L}}_1$, (52) as shown at the bottom of the page, can be obtained.

Similarly

$$\mathbb{E} \left[\hat{\mathbf{L}}_2 \right] = \mathbf{R}_2 + \frac{\mathbf{Q}_2}{2} = \mathbf{L}_2. \tag{53}$$

According to (52) and (53), the estimators are unbaised.

The proof of the weak consistency of the estimators are given as follows.

It can be seen from (45) and (48) that all samples of SOMD items $\nabla \mathbf{Z}_{12}$ in the sliding window are identical distribution, and the autocovariance of sequence $\nabla \mathbf{Z}_{12}$ is given as

$$\text{cov}(\nabla \mathbf{Z}_{12}(i), \nabla \mathbf{Z}_{12}(i+h))$$

$$\begin{aligned}
\mathbb{E} \left[\hat{\mathbf{L}}_1 \right] &= \frac{1}{4n} \left[\sum_{i=1}^n \mathbb{E} \left[\nabla \mathbf{Z}_{12}(i) \nabla \mathbf{Z}_{12}(i)^T \right] - \sum_{i=1}^n \mathbb{E} \left[\Delta \mathbf{Z}_2(i) \Delta \mathbf{Z}_2(i)^T \right] + \sum_{i=1}^n \mathbb{E} \left[\Delta \mathbf{Z}_1(i) \Delta \mathbf{Z}_1(i)^T \right] \right] \\
&= \frac{1}{4n} \left[n(2\mathbf{R}_1 + 2\mathbf{R}_2 + \mathbf{Q}_1 + \mathbf{Q}_2) - \sum_{i=1}^n [\Delta \mathbf{Z}(i) \Delta \mathbf{Z}(i)^T] - n(2\mathbf{R}_2 + \mathbf{Q}_2) + \sum_{i=1}^n [\Delta \mathbf{Z}(i) \Delta \mathbf{Z}(i)^T] + n(2\mathbf{R}_1 + \mathbf{Q}_1) \right] \\
&= \frac{2n(2\mathbf{R}_1 + \mathbf{Q}_1)}{4n} = \mathbf{R}_1 + \frac{\mathbf{Q}_1}{2} = \mathbf{L}_1 \tag{52}
\end{aligned}$$

$$= \begin{cases} 2(\mathbf{R}_1 + \mathbf{R}_2) + \mathbf{Q}_1 + \mathbf{Q}_2, & (h = 0) \\ -(\mathbf{R}_1 + \mathbf{R}_2), & (|h| = 1) \\ 0, & (|h| > 1) \end{cases} \tag{54}$$

which shows that sequence $\nabla \mathbf{Z}_{12}$ is weakly stationary.

Let

$$\mathbf{Y}_i = \nabla \mathbf{Z}_{12}(i) \nabla \mathbf{Z}_{12}(i)^T \tag{55}$$

$Y_{i,j,k}$ represent the j, k th entry of the matrix \mathbf{Y}_i , and let $\sigma_{j,k}^2 = \text{var}(Y_{i,j,k})$, which is finite, and let $\sigma^2 = \max_{j,k} \sigma_{j,k}^2$, which is finite as well. Then, for all j, k we have

$$\text{var} \left(\frac{1}{n} \sum_{i=1}^n Y_{i,j,k} \right) = \frac{1}{n^2} \sum_{i=1}^n \sum_{l=1}^n \text{cov}(Y_{i,j,k}, Y_{l,j,k}) \tag{56}$$

by stationarity. Thus, we have

$$\text{var} \left(\frac{1}{n} \sum_{i=1}^n Y_{i,j,k} \right) \leq \frac{3}{n} \sigma_{j,k}^2 \leq \frac{3\sigma^2}{n} \rightarrow 0 \tag{57}$$

as $n \rightarrow \infty$. By Markov's inequality, we have

$$\frac{1}{n} \sum_{i=1}^n \mathbf{Y}_i \xrightarrow{P} \mathbb{E}[\mathbf{Y}_i] \tag{58}$$

which shows that $\mu_{n2,\nabla Z_{12}}$ converges in probability to $\mu_{2,\nabla Z_{12}(k)}$, i.e.,

$$\mu_{n2,\nabla Z_{12}} \xrightarrow{P} \mu_{2,\nabla Z_{12}(k)}. \tag{59}$$

For the FOSD items $\Delta \mathbf{Z}_1$ and $\Delta \mathbf{Z}_2$, it can be seen from (45) that the first raw moments of them at each sampling moment is the difference of $\mathbf{Z}(t)$ at the same moment. Since the differences may be different at different sampling moment, i.e., $\Delta \mathbf{Z}(i) \neq \Delta \mathbf{Z}(j)$ ($i \neq j$), the sequences of $\Delta \mathbf{Z}_1$ and $\Delta \mathbf{Z}_2$ may not be weakly stationary. However, we can define $\Delta \mu_{n2}$ and $\Delta \mu_2$ as

$$\begin{cases} \Delta \mu_{n2} = \mu_{n2,\Delta Z_1} - \mu_{n2,\Delta Z_2} \\ = \frac{1}{n} \sum_{i=1}^n [\Delta \mathbf{Z}_1(i) \Delta \mathbf{Z}_1(i)^T - \Delta \mathbf{Z}_2(i) \Delta \mathbf{Z}_2(i)^T] \\ \Delta \mu_2 = \mu_{2,\Delta Z_1(k)} - \mu_{2,\Delta Z_2(k)}. \end{cases} \tag{60}$$

Let $\mathbf{Y}_i = \Delta \mathbf{Z}_1(i) \Delta \mathbf{Z}_1(i)^T - \Delta \mathbf{Z}_2(i) \Delta \mathbf{Z}_2(i)^T$, then the same argument used to obtain (59) can be used to show that $\Delta \mu_{n2}$ converges in probability to $\Delta \mu_2$, i.e.,

$$\Delta \mu_{n2} \xrightarrow{P} \Delta \mu_2. \tag{61}$$

Substitute $\Delta\mu_{n2}$ into (12) and (13), $\hat{\mathbf{L}}_1$ and $\hat{\mathbf{L}}_2$ can be rewritten in the following form:

$$\begin{cases} \hat{\mathbf{L}}_1 = \frac{\mu_{n2,\nabla Z_{12}} + \Delta\mu_{n2}}{4} \\ \hat{\mathbf{L}}_2 = \frac{\mu_{n2,\nabla Z_{12}} - \Delta\mu_{n2}}{4}. \end{cases} \quad (62)$$

It is noticed that $\hat{\mathbf{L}}_i$ (for $i = 1, 2$) are the linear function of consistent quantities. By the continuous mapping theorem, it can be concluded that the estimators $\hat{\mathbf{L}}_1$ and $\hat{\mathbf{L}}_2$ are consistent for \mathbf{L}_1 and \mathbf{L}_2 , respectively. ■

APPENDIX B PROOFS OF THEOREMS IN SECTION II-C

In this appendix, we provide the detailed proofs of Theorems 3 and 4 in Section II-C.

A. Proof of Theorem 3

Proof: According to (48), for any two different measurements processes $\mathbf{Z}_i(t)$ and $\mathbf{Z}_j(t)$ ($i \neq j$) from the n -independent measurements, the second raw moments of the SOMD item $\nabla\mathbf{Z}_{ij}(k)$ between them at time index k can be given as

$$\begin{aligned} \mu_{2,\nabla Z_{ij}(k)} &= \mathbb{E}[\nabla\mathbf{Z}_{ij}(k)\nabla\mathbf{Z}_{ij}(k)^T] \\ &= 2\mathbf{R}_i + 2\mathbf{R}_j + \mathbf{Q}_i + \mathbf{Q}_j. \end{aligned} \quad (63)$$

When all the equations about any two different measurements are stacked together, (64) as shown at the bottom of the page, can be obtained. By solving (64), (18) can be obtained.

B. Proof of Theorem 4

Proof: The proof of the unbiasedness of the estimator can be given as follows.

By the definition of $\mu_{n2,\nabla Z_{ij}}$ and (63), the following equation holds:

$$\begin{aligned} \mathbb{E}[\mu_{n2,\nabla Z_{ij}}] &= \frac{1}{n} \sum_{i=1}^n \mathbb{E}[\nabla\mathbf{Z}_{ij}(i)\nabla\mathbf{Z}_{ij}(i)^T] \\ &= \frac{1}{n} n(2\mathbf{R}_i + 2\mathbf{R}_j + \mathbf{Q}_i + \mathbf{Q}_j) \\ &= 2\mathbf{R}_i + 2\mathbf{R}_j + \mathbf{Q}_i + \mathbf{Q}_j. \end{aligned} \quad (65)$$

Then (66), as shown at the bottom of the page, can be obtained by taking the expectation of $\hat{\mathbf{L}}$, which shows that the estimator is unbiased

The proof of the consistency of the estimator can be given as follows.

For any two different measurement processes $\mathbf{Z}_i(t)$ and $\mathbf{Z}_j(t)$ ($i \neq j$), the first raw moments of SOMD item $\nabla\mathbf{Z}_{ij}(k)$ between them at time index k can be given as

$$\mu_{1,\nabla Z_{ij}(k)} = \mathbb{E}[\nabla\mathbf{Z}_{ij}(k)] = \mathbf{0}. \quad (67)$$

According to (63) and (67), all the samples of SOMD items $\nabla\mathbf{Z}_{ij}$ in the sliding window are identical distribution. In addition, the autocovariance of sequence $\nabla\mathbf{Z}_{ij}$ is independent of time index, which means that the sequence is weakly

$$\mathbf{A} \begin{bmatrix} \mathbf{R}_1 \\ \mathbf{R}_2 \\ \mathbf{R}_3 \\ \vdots \\ \mathbf{R}_n \end{bmatrix} = \frac{1}{2} \begin{bmatrix} \mu_{2,\nabla Z_{12}(k)} \\ \mu_{2,\nabla Z_{13}(k)} \\ \vdots \\ \mu_{2,\nabla Z_{1n}(k)} \\ \mu_{2,\nabla Z_{23}(k)} \\ \vdots \\ \mu_{2,\nabla Z_{2n}(k)} \\ \vdots \\ \vdots \\ \mu_{2,\nabla Z_{(n-1)n}(k)} \end{bmatrix} - \frac{1}{2} \begin{bmatrix} \mu_{2,\Delta\epsilon_1(k)} + \mu_{2,\Delta\epsilon_2(k)} \\ \mu_{2,\Delta\epsilon_1(k)} + \mu_{2,\Delta\epsilon_3(k)} \\ \vdots \\ \mu_{2,\Delta\epsilon_1(k)} + \mu_{2,\Delta\epsilon_n(k)} \\ \mu_{2,\Delta\epsilon_2(k)} + \mu_{2,\Delta\epsilon_3(k)} \\ \vdots \\ \mu_{2,\Delta\epsilon_2(k)} + \mu_{2,\Delta\epsilon_n(k)} \\ \vdots \\ \vdots \\ \mu_{2,\Delta\epsilon_{n-1}(k)} + \mu_{2,\Delta\epsilon_n(k)} \end{bmatrix}, \quad \mathbf{A} = \begin{bmatrix} \mathbf{I}_q & \mathbf{I}_q & \mathbf{I}_q \\ \mathbf{I}_q & \ddots & \mathbf{I}_q \\ \vdots & & \mathbf{I}_q \\ \mathbf{I}_q & \mathbf{I}_q & \mathbf{I}_q \\ \vdots & & \ddots \\ \mathbf{I}_q & & \mathbf{I}_q \\ \vdots & & \ddots \\ \vdots & & \mathbf{I}_q & \mathbf{I}_q \end{bmatrix}_{\frac{(n-1)q}{2} \times nq} \quad (64)$$

$$\mathbb{E}[\hat{\mathbf{L}}] = \frac{1}{2} \mathbf{A}^+ \begin{bmatrix} \mathbb{E}[\mu_{n2,\nabla Z_{12}}] \\ \mathbb{E}[\mu_{n2,\nabla Z_{13}}] \\ \vdots \\ \mathbb{E}[\mu_{n2,\nabla Z_{1n}}] \\ \mathbb{E}[\mu_{n2,\nabla Z_{23}}] \\ \vdots \\ \mathbb{E}[\mu_{n2,\nabla Z_{2n}}] \\ \vdots \\ \vdots \\ \mathbb{E}[\mu_{n2,\nabla Z_{(n-1)n}}] \end{bmatrix} = \frac{1}{2} \mathbf{A}^+ \left(\mathbf{A} \begin{bmatrix} 2\mathbf{R}_1 \\ 2\mathbf{R}_2 \\ 2\mathbf{R}_3 \\ \vdots \\ 2\mathbf{R}_n \end{bmatrix} + \begin{bmatrix} \mathbf{Q}_1 + \mathbf{Q}_2 \\ \mathbf{Q}_1 + \mathbf{Q}_3 \\ \vdots \\ \mathbf{Q}_{n-1} + \mathbf{Q}_n \end{bmatrix} \right) = \begin{bmatrix} \mathbf{R}_1 \\ \mathbf{R}_2 \\ \mathbf{R}_3 \\ \vdots \\ \mathbf{R}_n \end{bmatrix} + \frac{1}{2} \mathbf{A}^+ \begin{bmatrix} \mathbf{Q}_1 + \mathbf{Q}_2 \\ \mathbf{Q}_1 + \mathbf{Q}_3 \\ \vdots \\ \mathbf{Q}_{n-1} + \mathbf{Q}_n \end{bmatrix} = \mathbf{L} \quad (66)$$

stationary. Then by the same technique used to prove (59), we have

$$\boldsymbol{\mu}_{n2,\nabla\mathbf{Z}_{ij}} \xrightarrow{P} \boldsymbol{\mu}_{2,\nabla\mathbf{Z}_{ij}(k)}. \quad (68)$$

Moreover, it can be seen from (21) that $\hat{\mathbf{L}}$ is a linear function of consistent quantities. By the continuous mapping theorem, the estimator $\hat{\mathbf{L}}$ is consistent for \mathbf{L} . ■

REFERENCES

- [1] J. H. Kepper, B. C. Claus, and J. C. Kinsey, "A navigation solution using a MEMS IMU, model-based dead-reckoning, and one-way-travel-time acoustic range measurements for autonomous underwater vehicles," *IEEE J. Ocean. Eng.*, vol. 44, no. 3, pp. 664–682, Jul. 2019.
- [2] X. Li, W. Chen, C. Chan, B. Li, and X. Song, "Multi-sensor fusion methodology for enhanced land vehicle positioning," *Inf. Fusion*, vol. 46, pp. 51–62, Mar. 2019.
- [3] J. T. Jang, A. Santamaria-Navarro, B. T. Lopez, and A.-A. Agha-Mohammadi, "Analysis of state estimation drift on a MAV using PX4 autopilot and MEMS IMU during dead-reckoning," in *Proc. IEEE Aerosp. Conf.*, Big Sky, MT, USA, Mar. 2020, pp. 1–11.
- [4] M. Hilman, D. K. Basuki, and S. Sukaridhoto, "Virtual hand: VR hand controller using IMU and flex sensor," in *Proc. Int. Electron. Symp. Knowl. Creation Intell. Comput. (IES-KCIC)*, Bali, Indonesia, Oct. 2018, pp. 310–314.
- [5] P. Li, T. Qin, B. Hu, F. Zhu, and S. Shen, "Monocular visual-inertial state estimation for mobile augmented reality," in *Proc. IEEE Int. Symp. Mixed Augmented Reality (ISMAR)*, Nantes, France, Oct. 2017, pp. 11–21.
- [6] T. L. Grigorie, R. M. Botez, D. G. Sandu, and O. Grigorie, "Experimental testing of a data fusion algorithm for miniaturized inertial sensors in redundant configurations," in *Proc. Int. Conf. Math. Methods, Math. Models Simulation Sci. Eng.*, Interlaken, Switzerland, Feb. 2014, pp. 116–122.
- [7] J.-O. Nilsson and I. Skog, "Inertial sensor arrays— A literature review," in *Proc. Eur. Navigat. Conf. (ENC)*, Helsinki, Finland, May 2016, pp. 1–10.
- [8] A. Waegli, S. Guerrier, and J. Skaloud, "Redundant MEMS-IMU integrated with GPS for performance assessment in sports," in *Proc. IEEE/ION Position, Location Navigat. Symp.*, Monterey, CA, USA, May 2008, pp. 1260–1268.
- [9] I. Colomina, M. Giménez, J. Rosales, M. Wis, A. Gómez, and P. Miguelanz, "Redundant IMUs for precise trajectory determination," in *Proc. XXth ISPRS Congr.*, Istanbul, Turkey, Jul. 2004, p. 17.
- [10] J. B. Bancroft, "Multiple IMU integration for vehicular navigation," in *Proc. ION GNSS*, Savannah, GA, USA, Sep. 2009, pp. 1828–1840.
- [11] K. Eckenhoff, P. Geneva, and G. Huang, "Sensor-Failure-Resilient multi-IMU visual-inertial navigation," in *Proc. Int. Conf. Robot. Autom. (ICRA)*, Montreal, QC, Canada, May 2019, pp. 3542–3548.
- [12] M. Zhang, X. Xu, Y. Chen, and M. Li, "A lightweight and accurate localization algorithm using multiple inertial measurement units," *IEEE Robot. Autom. Lett.*, vol. 5, no. 2, pp. 1508–1515, Apr. 2020.
- [13] J. B. Bancroft and G. Lachapelle, "Data fusion algorithms for multiple inertial measurement units," *Sensors*, vol. 11, no. 7, pp. 6771–6798, 2011.
- [14] A. Waegli, J. Skaloud, S. Guerrier, M. E. Parés, and I. Colomina, "Noise reduction and estimation in multiple micro-electro-mechanical inertial systems," *Meas. Sci. Technol.*, vol. 21, no. 6, 2010, Art. no. 065201.
- [15] S. Guerrier, "Integration of skew-redundant MEMS-IMU with GPS for improved navigation performance," M.S. thesis, École Polytechnique Fédérale de Lausanne (EPFL), Lausanne, Switzerland, Jun. 2008.
- [16] T. Bollerslev, "Generalized autoregressive conditional heteroskedasticity," *J. Econ.*, vol. 31, no. 3, pp. 307–327, 1986.
- [17] S. Gao, Y. Zhong, and W. Li, "Random weighting method for multi-sensor data fusion," *IEEE Sensors J.*, vol. 11, no. 9, pp. 1955–1961, Sep. 2011.
- [18] M. R. Velázquez, L. Latorre, F. Mailly, and P. Nouet, "A new algorithm for fault tolerance in redundant sensor systems based on real-time variance estimation," *IEEE Sensors J.*, vol. 22, no. 15, pp. 15410–15418, Aug. 2022.
- [19] C. R. Rao, "Estimation of heteroscedastic variances in linear models," *J. Amer. Stat. Assoc.*, vol. 65, no. 329, pp. 161–172, Mar. 1970.
- [20] H. Zhang, Y. Chang, and H. Che, "Measurement-based adaptive Kalman filtering algorithm for GPS/INS integrated navigation system," *J. Chin. Inertial Technol.*, vol. 18, no. 6, pp. 696–701, 2010.
- [21] Q. Zhou, H. Zhang, and Y. Wang, "A redundant measurement adaptive Kalman filter algorithm," *Acta Aeronaut. Astronaut. Sinica*, vol. 36, no. 5, pp. 1596–1605, 2015.
- [22] Z. Li, H. Zhang, Q. Zhou, and H. Che, "An adaptive low-cost INS/GNSS tightly-coupled integration architecture based on redundant measurement noise covariance estimation," *Sensors*, vol. 17, no. 9, p. 2032, Sep. 2017.
- [23] L. Jiang and H. Zhang, "Redundant measurement-based second order mutual difference adaptive Kalman filter," *Automatica*, vol. 100, pp. 396–402, Feb. 2019.
- [24] B. Ge, H. Zhang, L. Jiang, Z. Li, and M. M. Butt, "Adaptive unscented Kalman filter for target tracking with unknown time-varying noise covariance," *Sensors*, vol. 19, no. 6, p. 1371, Mar. 2019.
- [25] K. Zhu et al., "MIMU/odometer fusion with state constraints for vehicle positioning during BeiDou signal outage: Testing and results," *Sensors*, vol. 20, no. 8, p. 2302, 2020.
- [26] S. Guerrier, J. Skaloud, Y. Stebler, and M.-P. Victoria-Feser, "Wavelet-variance-based estimation for composite stochastic processes," *J. Amer. Statist. Assoc.*, vol. 108, no. 503, pp. 1021–1030, 2013.
- [27] Y. Zhang, D. A. Cucci, R. Molinari, and S. Guerrier, "Scale-wise variance minimization for optimal virtual signals: An approach for redundant gyroscopes," *IEEE Trans. Signal Process.*, vol. 70, pp. 5320–5333, 2022.



Hongliang Huang was born in Kaifeng, Henan, China, in 1989. He received the B.S. degree in measurement control technology and instruments from Zhengzhou University, Zhengzhou, China, in 2013, and the M.S. degree in mechanical engineering from the University of Science and Technology Beijing, Beijing, China, in 2016. He is currently pursuing the Ph.D. degree in control theory and control engineering with Beihang University, Beijing, China.

His research interests include Kalman filtering, state estimation, and visual inertial integrated navigation.



Hai Zhang received the B.S., M.S., and Ph.D. degrees in system engineering from Northwestern Polytechnical University, Xi'an, China, in 1992, 1995, and 1998, respectively.

From 1998 to 2001, he was a Postdoctoral Research Fellow with Beihang University, Beijing, China. Since 2001, he has been an Assistant Professor with the School of Automation Science and Electrical Engineering, Beihang University. His research interests include optimal estimation, inertial navigation, visual navigation, and integrated navigation.



Liuyang Jiang received the B.S. degree in measurement control technology and instruments from the Qingdao University of Technology, Qingdao, China, in 2008, the M.S. degree in control theory and control engineering from the Shandong University of Science and Technology, Qingdao, in 2012, and the Ph.D. degree in control theory and control engineering from Beihang University, Beijing, China, in 2020.

Since 2021, she has been a Lecturer with the School of Information and Control Engineering, Qingdao University of Technology. Her research interests include adaptive Kalman filtering, state estimation, and stochastic systems.